

## Supplementary Information

# Revealing the electrochemical Peltier heat of microbial direct extracellular electron transfer

Benjamin Korth<sup>[a]</sup>, Thomas Maskow<sup>[a]</sup>, Cristian Picioareanu<sup>[b]</sup> and Falk Harnisch<sup>[a]</sup>

[a] Dipl.-Biochem. B. Korth, PD Dr. T. Maskow, Dr. F. Harnisch, Department of Environmental Microbiology, Helmholtz-Centre for Environmental Research, Permoserstr. 15, 04275 Leipzig (Germany), E-mail: [falk.harnisch@ufz.de](mailto:falk.harnisch@ufz.de) (F. Harnisch)

[b] AssocProf. Dr. C. Picioareanu, Department of Biotechnology, Faculty of Applied Sciences, Delft University of Technology, Julianalaan 67, 2628 BC Delft (The Netherlands)

## Content

1	List of Symbols.....	2
2	Validation of the bioelectrocalorimeter and control experiments.....	4
2.1	General conditions .....	4
2.2	Validation of the bioelectrocalorimeter using the redox couple $K_3[Fe(CN)_6]/K_4[Fe(CN)_6]$ .....	4
2.2.1	Calorimetric measurement of the electrochemical Peltier heat.....	4
2.2.2	Determination of the molar electrochemical Peltier heat $\overline{J}$ .....	4
2.2.3	Experimental setup of the inorganic control experiments .....	5
2.2.4	Baseline correction of the heat production rate .....	6
2.2.5	Calculating the molar electrochemical Peltier heat .....	6
2.2.6	$I \times R$ drop correction at the working electrode .....	7
2.2.7	Formal potential of the redox couple $K_3[Fe(CN)_6]/K_4[Fe(CN)_6]$ .....	7
2.3	Control experiment for excluding heat produced at the counter electrode.....	8
2.4	Position calibration of the 2 <sup>nd</sup> reference electrode for measurement of the Joule heating contributing to the heat production rate of the bioelectrocalorimeter .....	10
3	Experimental procedure for the determination of the microbial electrochemical Peltier heat .....	11
3.1	Setup of the bioelectrocalorimeter.....	11
3.2	Cultivation of biofilm anodes .....	11
3.3	Inoculation of the bioelectrocalorimeter and medium exchange .....	11
3.4	Calorimetric measurement .....	11
4	Calculations.....	11
4.1	Identifying the heat sources within a bioelectrocalorimeter.....	11
4.2	Joule heating .....	11
4.3	Overpotential heating .....	12
4.4	Catabolic heat due to acetate oxidation .....	12
4.5	Anabolic heat.....	13
4.6	Theoretical heat production rate.....	13
4.7	$I \times R$ drop correction of the working electrode potential.....	13
4.8	Statistical evaluation of the redox titration experiments .....	13
5	Characterization of biofilm anodes.....	13
5.1	Cyclic voltammetry .....	13
5.2	T-RFLP genetic analysis .....	14
5.3	Current densities during chronoamperometry experiments .....	14
6	References.....	15

# 1 List of Symbols

**Table S1** List of symbols used in the main article and in the supplementary information

Symbol	Unit	Description
<i>Calorimetric parameters</i>		
$P$	W	Monitored heat production rate
$P_{\text{Baseline}}$	W	Heat production rate of the non-electrochemical and non-biological thermal effects, i.e. baseline at open circuit potential (zero current flow)
$m$	s <sup>-1</sup>	Slope in the linear equation for the baseline correction of the heat production rate
$n$	W	Offset in the linear equation for the baseline correction of the heat production rate
$P_{\text{Heat}}$	W	Measured heat production rate of the electrochemical and biological effects corrected by $P_{\text{Baseline}}$
$P_{\text{Joule}}$	W	Calculated heat production rate caused by the Joule heating within the reactor vessel, between working electrode and 2 <sup>nd</sup> reference electrode (being placed outside the calorimeter but in ionic contact)
$P_{\text{Over}}$	W	Calculated heat production rate caused by the applied overpotential at the working electrode
$P_{\text{ePh}}$	W	Heat production rate by the electrochemical Peltier effect
$P_{\text{Cat}}$	W	Calculated heat production rate in catabolism, resulting from the anaerobic oxidation of acetate by the biofilm anodes
$P_{\text{Ana}}$	W	Heat production rate in anabolism, caused by the build-up of biomass from acetate and maintenance processes
$P_{\text{Theory}}$	W	Theoretical heat production rate summing up the calculated values of $P_{\text{Joule}}$ , $P_{\text{Over}}$ and $P_{\text{Cat}}$
$P_{\text{mePh}}$	W	Heat production rate by the microbial electrochemical Peltier effect
$P_{\text{Electro}}$	W	Heat production rate of electrochemical processes, summing up $P_{\text{Joule}}$ , $P_{\text{Over}}$ and $P_{\text{mePh}}$
<i>Electrochemical parameters</i>		
$E$	V	Potential of the working electrode vs. standard hydrogen electrode (SHE) without $I \times R$ drop correction
$E_{\text{WE}}$	V	Potential of the working electrode vs. standard hydrogen electrode (SHE) and corrected for the $I \times R$ drop
$E_{\text{IR drop}}$	V	Potential drop at the working electrode caused by the $I \times R$ drop
$E_{\text{joule}}$	V	Potential between the working electrode and the 2 <sup>nd</sup> reference electrode needed to calculate $P_{\text{Joule}}$
$E_{\text{Onset}}$	V	Onset potential of the bioelectrocatalytic reaction
$E_{\text{EET}}^f$	V	Formal potential of the extra cellular electron transfer-site of a biofilm anode
$E_{\text{Fe}}^f$	V	Formal potential of the redox couple $\text{K}_3[\text{Fe}(\text{CN})_6]/\text{K}_4[\text{Fe}(\text{CN})_6]$
$\eta$	V	Potential difference (overpotential) between $E_{\text{WE}}$ and $E_{\text{Onset}}$ in biological experiments and between $E_{\text{WE}}$ and $E_{\text{Fe}}^f$ in inorganic experiments
$I$	A	Current
$j$	mAc <sup>m</sup> - <sup>2</sup>	Current density per projected surface area
$R_{\text{joule}}$	Ω	Electrolyte resistance between working electrode and 2 <sup>nd</sup> reference electrode
$R_{\text{IR drop}}$	Ω	Electrolyte resistance used to calculate the $I \times R$ drop between working and reference electrode

$E_0, E_1, E_2$	V	Start potential and vertex potentials during cyclic voltammetry, respectively
$F$	Cmol <sup>-1</sup>	Faraday constant (96485.34 C mol <sup>-1</sup> )
$z$	-	Number of transferred electrons per reaction
$v$	mVs <sup>-1</sup>	Scan rate during cyclic voltammetry
$R$	$\Omega$	Electrolyte resistance used to calculate the $I \times R$ drop
$\sigma$	mScm <sup>-1</sup>	Ionic conductivity of electrolyte solutions

---

*Thermodynamic parameters*

---

$\Delta_f H^0$	kJmol <sup>-1</sup>	Enthalpy of formation in standard conditions (298.15 K, 101.325 kPa)
$\Delta_R H^0$	kJmol <sup>-1</sup>	Enthalpy of reaction in standard conditions
$\Delta_R H_{Electrons}^0$	kJmol <sub>e</sub> <sup>-1</sup>	Enthalpy of reaction per transferred electron in standard conditions
$r_{AC}$	mol <sub>e</sub> -s <sup>-1</sup>	Rate of anaerobic acetate oxidation normalized to transferred moles of electrons
$\Delta_f G^{0'}$	kJmol <sup>-1</sup>	Gibbs energy of formation in biological standard conditions (pH 7, 298.15 K, 101.325 kPa)
$\Delta_R G^{0'}$	kJmol <sup>-1</sup>	Gibbs energy of reaction in biological standard conditions
$\Delta_R G$	kJmol <sup>-1</sup>	Gibbs energy of reaction corrected for temperature and concentrations
$\Pi$	kJmol <sup>-1</sup>	Molar electrochemical Peltier heat
$\Pi_m$	kJmol <sup>-1</sup>	Molar microbial electrochemical Peltier heat
$\Pi_{Oxidation}$	kJmol <sup>-1</sup>	Molar electrochemical Peltier heat for the oxidation reaction of K <sub>4</sub> [Fe(CN) <sub>6</sub> ]
$\Pi_{Reduction}$	kJmol <sup>-1</sup>	Molar electrochemical Peltier heat for the reduction reaction of K <sub>3</sub> [Fe(CN) <sub>6</sub> ]
$U$	J	Internal energy
$Q$	J	Heat
$W$	J	Work
$Q_{rev}$	J	Heat of reversible processes
$S$	JK <sup>-1</sup>	Entropy
$H$	J	Enthalpy
$p$	kgm <sup>-1</sup> s <sup>-2</sup>	Pressure
$V$	m <sup>3</sup>	Volume
$T$	K	Temperature
$R$	Jmol <sup>-1</sup> K <sup>-1</sup>	Gas constant (being 8.314 Jmol <sup>-1</sup> K <sup>-1</sup> )

---

*Miscellaneous*

---

$L$	cm	Distance between working electrode and reference electrode
$t$	s	Time

---

## 2 Validation of the bioelectrocalorimeter and control experiments

### 2.1 General conditions

All chemicals were of analytical or biochemical grade (from Sigma-Aldrich Corp., U.S.A. and Merck KGaA, Germany) and used as received. All potential values in the main article and in the supplementary information (SI) are provided versus standard hydrogen electrode (SHE) and corrected for the respective  $i \times R$  drop (SI 2.2.6 and 4.7).

### 2.2 Validation of the bioelectrocalorimeter using the redox couple $K_3[Fe(CN)_6]/K_4[Fe(CN)_6]$

To validate the in-house developed bioelectrocalorimeter, experiments with a well-studied inorganic redox couple  $K_3[Fe(CN)_6]/K_4[Fe(CN)_6]$  were performed and results compared with data available in literature. For the validation experiments the reactor calorimeter was considered as electrocalorimeter (Scheme S1)

#### 2.2.1 Calorimetric measurement of the electrochemical Peltier heat

According to Vetter and Agar the electrochemical Peltier heat is defined as the heat produced or absorbed at an electrode/ electrolyte interface when an electron is reversibly transferred through this interface at constant temperature and pressure.<sup>1, 2</sup> To fulfil these conditions, it is convenient to use the internal energy definition according to the first law of thermodynamics (equation 1):

$$dU = \delta Q + \delta W \quad (1)$$

As the produced/ consumed heat of the electrode reactions is small compared to the large heat capacity of the bioelectrocalorimeter, it only causes a very small temperature change of the measurement solution. The heat transition can therefore be regarded as reversible and hence according to Clausius' entropy definition, the heat of a reversible and isothermal process is defined as:

$$\frac{\delta Q_{rev}}{T} = dS \quad (2)$$

Replacing in equation 1 the heat  $\delta Q$  with the entropy from equation 2 and the general work  $\delta W$  with the volume work  $pdV$  yields the following equation 3:

$$dU = TdS - pdV \quad (3)$$

Following this, the entropy and the enthalpy  $dH = dU + pdV + Vdp$  can be linked:<sup>3</sup>

$$dH = TdS + Vdp \quad (4)$$

For an isobaric process it only remains the relation (equation 5):

$$dH = TdS \quad (5)$$

This clearly shows that for the conditions in the bioelectrocalorimeter, the enthalpy and the entropy are linked, and thus the measured heat can be related to the entropic electrochemical Peltier heat effect.<sup>2</sup>

#### 2.2.2 Determination of the molar electrochemical Peltier heat $\Pi$

The main heat fluxes within the electrocalorimeter are : (i) Joule heat flux ( $P_{Joule}$ ), (ii) overpotential heat flux ( $P_{Over}$ ) and (iii) the heat flux due to the electrochemical Peltier heat ( $P_{ePh}$ ) already mentioned in the main article (see Fig. 2). Another potential heat source is the electronic Peltier heat flux at the electrode/ wire interface but this effect is several orders of magnitude smaller than the others and thus can be neglected (e.g.  $-5.3 \mu VK^{-1}$  for platinum and  $9.1 \mu VK^{-1}$  for titanium at 300 K).<sup>4, 5</sup> The total heat flux ( $P_{Heat}$ ) during the calorimetric experiment is then composed of the heat contributions (i-iii):

$$P_{Heat} = P_{Joule} + P_{Over} + P_{ePh} \quad (6)$$

$$P_{Joule} = IR_{Joule}^2 \quad (7)$$

$$P_{Over} = \eta I \quad (8)$$

$$P_{ePh} = \frac{\Pi}{zF} I \quad (9)$$

$\Pi$  is the molar electrochemical Peltier heat ( $\text{Jmol}^{-1}$ ),  $z$  the number of transferred electrons per reaction,  $F$  the Faraday constant ( $\text{Cmol}^{-1}$ ),  $\eta$  the overpotential (V),  $I$  the current and  $R_{\text{Joule}}$  the resistance ( $\Omega$ ) between the working electrode and the 2<sup>nd</sup> reference electrode. The Joule heating (equation 7) and overpotential heating (equation 8) are generally exothermic processes and thus were considered to possess negative values by thermodynamic convention. In contrast, the electrochemical Peltier heat (equation 9) is defined as positive for an exothermic anodic reaction and negative for an endothermic cathodic reaction.<sup>4</sup>

$$P_{\text{Heat}} = -R_{\text{Joule}}I^2 - \eta I - \frac{\Pi|I|}{zF} \quad (10)$$

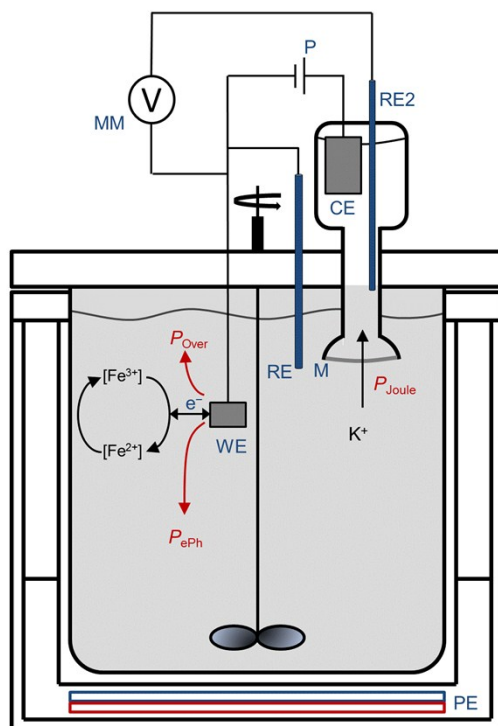
By normalizing to the current ( $I$ ) equation 10 is transformed in a linear relationship (equation 11):

$$\frac{P_{\text{Heat}}}{|I|} + |\eta| = -R_{\text{Joule}}|I| - \frac{\Pi}{zF} \quad (11)$$

Based on equation 11 the molar electrochemical Peltier is obtained from the intercept of the plot (see Figure S2 in the supplementary information and Figure 2 in the main article).

### 2.2.3 Experimental setup of the inorganic control experiments

The experiments were conducted in a reactor calorimeter immersed in a thermostated liquid bath of propylene glycol (CPA202, Syrris Ltd, UK) developed to accurately measure heat fluxes and tailored to serve as bioelectrocalorimeter in this study (Scheme 1 of the main article). A three-electrode setup was integrated into the calorimetric reaction vessel ( $V = 250$  mL) and controlled by a potentiostat (VSP-300, Bio-Logic SAS, France). The working (WE) and the counter (CE) electrode consisted of a titanium-wired platinum foil (Goodfellow GmbH, Germany, WE:  $1.2 \times 0.8 \text{ cm} \times 0.125 \text{ mm}$ , CE:  $1.4 \text{ cm} \times 4.4 \text{ cm} \times 0.125 \text{ mm}$ ). The reference electrode (Ag/AgCl with saturated KCl,  $-0.197$  V vs. SHE, SE 10, Meinsberg Sensortechnik GmbH, Germany) was placed at a distance of 3 cm to the working electrode. The counter electrode was spatially separated from the working electrode compartment and localized outside the calorimetric reactor vessel (Scheme S1). The counter electrode compartment consisted of a glass vessel on the top of the reactor vessel and a banana-shaped glass vessel within the reactor vessel. Both were connected using a flexible tube (Tygon® R-3603, Saint-Gobain Performance Plastics Corporation, France). The resulting total working volume of the counter electrode compartment was 11.5 mL. Working electrode and counter electrode compartment were physically separated but ionically connected with a glued (S78pp, RECA NORM GmbH, Germany) cation exchange membrane (fumasep®FKE, FuMA-Tech GmbH, Germany) at the bottom of the banana-shaped glass vessel ( $A_{\text{Membrane}} = 4 \text{ cm}^2$ ). To verify that the reactions and possible thermal effects occurring at the counter electrode do not influence the measurement of the heat production rate of the working electrode, control experiments with an additional working electrode compartment were performed (SI 2.3). An additional 2<sup>nd</sup> reference electrode (Ag/AgCl,  $3 \text{ molL}^{-1}$  KCl,  $-0.210$  V vs. SHE, Flexref, World Precision Instruments Inc., U.S.A.) was inserted into the counter electrode compartment for measuring of Joule heating (SI 4.2). To identify the correct position of the 2<sup>nd</sup> reference electrode a position calibration was performed (SI 2.4). The solution was composed of  $50 \text{ mmolL}^{-1}$   $\text{K}_3[\text{Fe}(\text{CN})_6]$  and  $50 \text{ mmolL}^{-1}$   $\text{K}_4[\text{Fe}(\text{CN})_6]$ . The counter electrode compartment was filled with the same solution. The  $\text{K}_3[\text{Fe}(\text{CN})_6]/\text{K}_4[\text{Fe}(\text{CN})_6]$  experiments were conducted at  $25$  °C to have similar conditions compared to reference data.<sup>4</sup> The reaction calorimeter was operated with the ChemiCall V1 software (Syrris Ltd, UK). The heat production rate was recorded every 10 s in the isoperibolic measuring mode. The reactor volume was stirred with 50 rpm. After recording a heat production rate baseline (SI 2.2.4), chronoamperometry experiments were conducted (SI 2.2.5).



**Scheme S1.** Illustration of the electrocalorimeter and a simplified flow of redox species, electrons, ions and heat:  $K_3[Fe(CN)_6]/K_4[Fe(CN)_6]$  is reduced/ oxidized at the working electrode. The grey shaded area of the reactor contributed to the heat flux that was dissipated and recorded by the Peltier element which acted as the actual heat sensor. Heat is produced due to the irreversible processes Joule heating ( $P_{Joule}$ ) and overpotential heating ( $P_{Over}$ ) and the reversible electrochemical Peltier heat ( $P_{ePh}$ ). WE: Working electrode, CE: Counter electrode, RE: Reference electrode (Ag/AgCl sat. KCl), RE2: 2<sup>nd</sup> reference electrode (Ag/AgCl 3.0 molL<sup>-1</sup> KCl), M: Cation exchange membrane, MM: Multimeter, P: Potentiostat, PE: Peltier element.

## 2.2.4 Baseline correction of the heat production rate

The thermal effects of the bioelectrochemical processes ( $P_{Heat}$ ) can be easily separated from the monitored heat production rate  $P$  by using a baseline correction (equation 12). The baseline comprises all non-bioelectrochemical effects like water evaporation, friction heat from stirring, unspecific diffusion driven ion transport through the membrane and the undefined heat exchange with the surrounding. For the definition of the baseline the heat production rate before and after a bioelectrochemical experiment (each time for 5 min) was assessed and linearly interpolated (equation 13). Here,  $m$  and  $n$  were the slope and the offset of the linearly assumed baseline, respectively.

$$P_{Heat} = P - P_{Baseline} \quad (12)$$

$$P_{Baseline} = mt + n \quad (13)$$

## 2.2.5 Calculating the molar electrochemical Peltier heat

After recording a heat production rate baseline, redox titrations were performed. Several chronoamperometric experiments (for reduction reactions: from  $E_{WE} = 0.26$  V to  $E_{WE} = 0.40$  V and for oxidation reactions: from  $E_{WE} = 0.46$  V to  $E_{WE} = 0.50$  V) were conducted consecutively interrupted by open circuit potential to reach again the baseline level of the heat production rate. Representative examples of these oxidation/ reduction experiments can be seen in Figure S1. Oxidation and reduction experiments were alternately conducted to keep the relative concentration of the redox species at a constant level and hence to maintain the formal potential. During oxidative conditions (Figure S1) both current density ( $j$ ) and the heat production rate ( $P_{Heat}$ ) increased with more positive potentials, whereas in the reduction experiments current density ( $j$ ) decreased and heat production rate ( $P_{Heat}$ ) increased with more negative potentials (Figure 2A in the main article). The last 50 measured points (i.e. 300 seconds) of each potential step (while steady state) were taken to calculate the respective current, working electrode potential and heat production rate. With these values and the method described in SI 2.2.2 a plot for determining the molar electrochemical Peltier heat was obtained (Figure 2B in the main article). Based on the linear equations shown in Figure 2B in the main article the molar electrochemical Peltier heats  $\int j_{Oxidation} = -47 \pm 11$  kJmol<sup>-1</sup> and  $\int j_{Reduction} = 46 \pm 12$  kJmol<sup>-1</sup> were derived, which were in accordance to the literature value  $\int j_{Ox/Red} = \pm 45$  kJmol<sup>-1</sup>.<sup>4</sup>

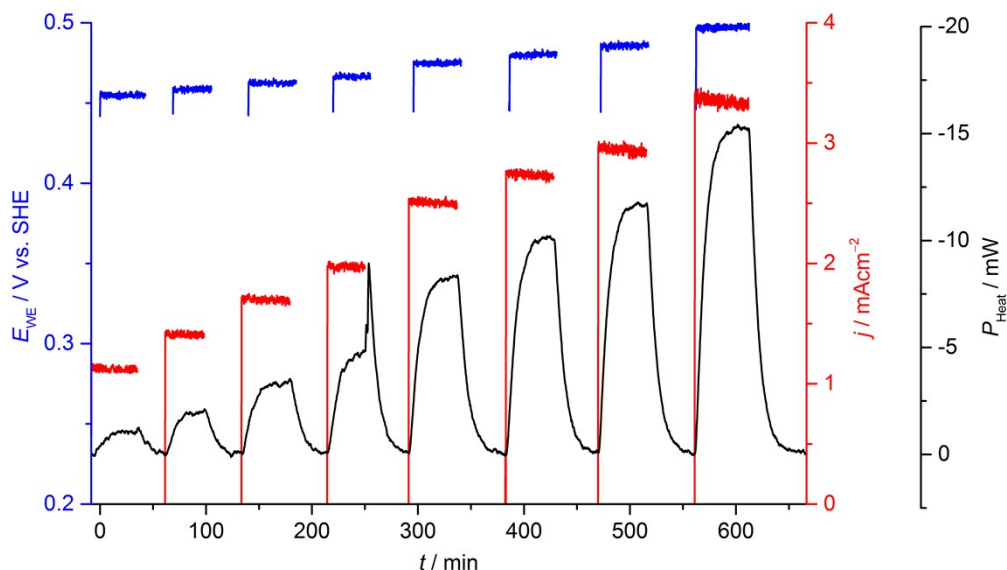


**Figure S1.** Example of an oxidation experiment with  $\text{K}_3[\text{Fe}(\text{CN})_6]/\text{K}_4[\text{Fe}(\text{CN})_6]$ . At oxidative potentials, the current density ( $j$ ) and heat production rate ( $P_{\text{heat}}$ ) increased with more positive potentials ( $E_{\text{WE}}$ ). Steady state values of every single potential step were used for further calculations.

### 2.2.6 $I \times R$ drop correction at the working electrode

In the reactor the working electrode and the reference electrode were 3 cm apart from each other. A potential drop between the reference electrode and the working electrode occurred due to the limited ionic conductivity of the solution and was calculated using Ohm's law:

$$E_{IR \text{ drop}} = IR_{IR \text{ drop}} \quad (14)$$

Subsequently the working electrode potential was corrected for this ohmic potential drop:

$$E_{\text{WE}} = E - E_{IR \text{ drop}} \quad (15)$$

The specific electrolyte resistance  $R_{IR \text{ drop}}$  was calculated using the distance between working and reference electrode ( $L = 3 \text{ cm}$ ) and conductivity  $\sigma$  of the solution. The conductivity was measured with a conductivity meter (Seven Excellence S470, Mettler-Toledo GmbH, Germany) and a value of  $\sigma = 32 \text{ mS cm}^{-1}$  was estimated for a  $50 \text{ mmol L}^{-1}$   $\text{K}_3[\text{Fe}(\text{CN})_6]/\text{K}_4[\text{Fe}(\text{CN})_6]$  solution at  $25 \text{ }^\circ\text{C}$  and a stirring speed of 50 rpm.

$$R_{IR \text{ drop}} = \frac{1}{\sigma \times L} = \frac{1}{32 \frac{\text{mS}}{\text{cm}} \times 3 \text{ cm}} = 10.4 \Omega \quad (16)$$

Unless otherwise specified, all reported working electrode potential values in the main article and the supplementary information were corrected for the  $I \times R$  drop.

### 2.2.7 Formal potential of the redox couple $\text{K}_3[\text{Fe}(\text{CN})_6]/\text{K}_4[\text{Fe}(\text{CN})_6]$

To avoid contributions from heat produced at the counter electrode, this electrode was spatially separated from the working electrode and was located outside of the reactor vessel (Scheme S1 and SI 2.3). This required setup caused a large electrolyte resistance between working and counter electrode. Although it was possible to execute chronoamperometry with  $\text{K}_3[\text{Fe}(\text{CN})_6]/\text{K}_4[\text{Fe}(\text{CN})_6]$ , the cyclic voltammetry (needed to estimate the formal potential of the redox couple) was not feasible. Therefore, a comparable experiment in a three-neck round-bottom flask was conducted with the same distance between the working and reference electrode but a smaller distance between working and counter electrode. The solution was the same as in SI 2.2.3 and the temperature was adjusted to be  $25 \text{ }^\circ\text{C}$ . Cyclic voltammetry was performed ( $E_0 = 0.2 \text{ V}$ ,  $E_1 = 0.7 \text{ V}$ ,  $E_2 = 0.2 \text{ V}$ ,  $\nu = 1 \text{ mVs}^{-1}$ ,  $n = 3$ , working electrode potentials not corrected for  $I \times R$  drop). The calculation of the first derivative (Figure S3 inset) of the voltammogram (Figure S3) allowed identifying the formal potential  $E_{\text{Fe}}^{\text{f}} = 0.44 \text{ V}$  of the redox couple  $\text{K}_3[\text{Fe}(\text{CN})_6]/\text{K}_4[\text{Fe}(\text{CN})_6]$ , which was in accordance with literature ( $E_{\text{Fe}}^{\text{f}} = 0.36 \text{ V}$ ) with respect to the overpotential.<sup>6</sup>

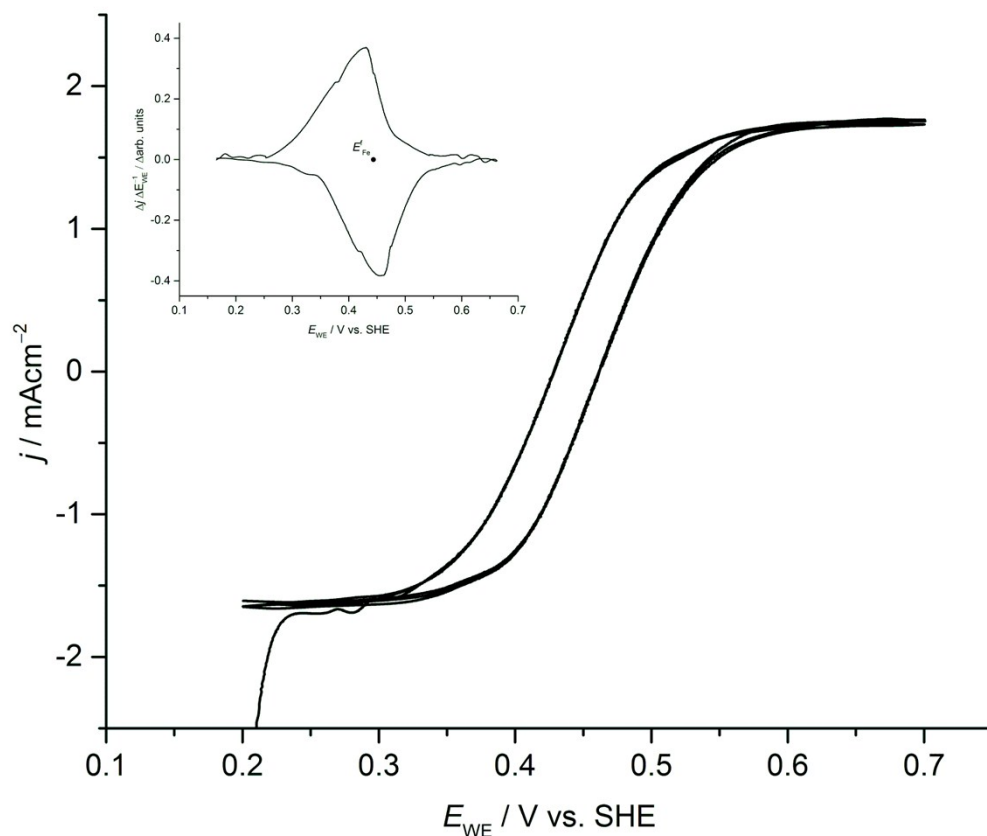
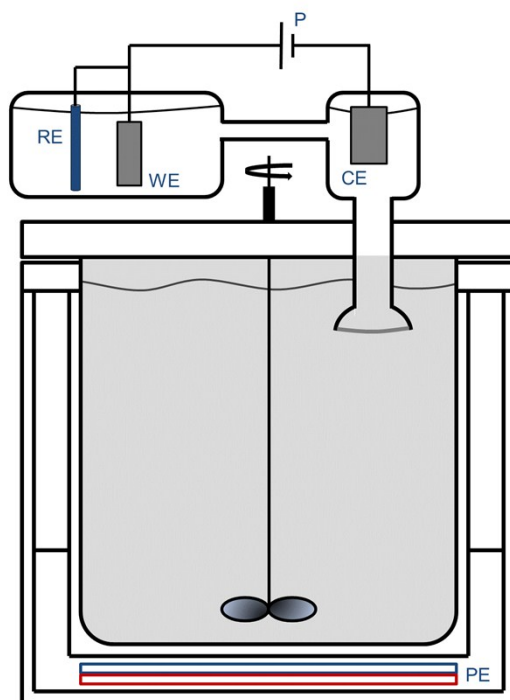


**Figure S3.** Cyclic voltammogram of the redox couple  $K_3[Fe(CN)_6]/K_4[Fe(CN)_6]$  in a three-neck round-bottom flask for deriving the formal potential of this couple. The inset shows the first derivative of the third cycle corrected by the  $i \times R$  drop. The mean value of the anodic and cathodic peak revealed a formal potential of  $E'_{Fe} = 0.44$  V being in accordance to literature.<sup>6</sup>

### 2.3 Control experiment for excluding heat produced at the counter electrode

In the bioelectrocalorimeter the redox reaction at the counter electrode led to an unavoidable heat flux in the calorimetric setup, which needed to be discerned from the heat flux at the working electrode. To verify that heat flux occurring at the counter electrode did not influence the measurement in the working electrode compartment the experimental setup was supplemented with an additional reaction vessel at the top of the reactor lid for hosting the working electrode (Scheme S2). Working ( $2.0 \times 2.0$  cm-sized titanium-wired platinum foil; Goodfellow GmbH, Germany) and reference electrode were now located in this new compartment which was ionically connected via a tube (Tygon® R-3603, Saint-Gobain Performance Plastics Corporation, France) to the counter electrode compartment (Scheme S2). The further experimental setup was kept identical. The bioelectrocalorimeter vessel was filled with 200 mL medium used for the biological experiments as well as the counter electrode compartment and the new working electrode compartment. The heat production rate was monitored every 10 s in the isoperibolic measuring mode at 35 °C, while stirring with 50 rpm. After recording a baseline for the heat production rate  $P_{Heat}$  galvanostatic experiments were performed. A current of 4 mA was applied for 20 hours to the working electrode simulating a representative current flow as achieved in the bioelectrocalorimetric experiments (Figure 1 in the main article) and thus representative heat evolution at the counter electrode. Approximately 40 V were applied to the working electrode and -11 V were applied to the counter electrode.  $P_{Heat}$  of the anodic compartment was not affected by the reduction reactions at the counter electrode and the  $P_{Heat}$  baseline remained at  $-1.91 \pm 0.04$  mW during the experiment (Figure S4). After ca. 12.5 h the current production collapsed, probably due to bubble formation that block the ionic path in the connecting tube. Most importantly  $P_{Heat}$  was not affected for either current flow or no current flow (Figure S4).



**Scheme S2.** Illustration of the electrocalorimeter setup with the supplemented reaction vessel at the top of the reactor lid to simulate similar counter electrode processes compared to biological experiments. The grey shaded area of the reactor contributed to the heat flux that was dissipated and recorded by the Peltier element which acted as the actual heat sensor. WE: Working electrode, CE: Counter electrode, RE: Reference electrode (Ag/AgCl sat. KCl), P: Potentiostat, PE: Peltier element.

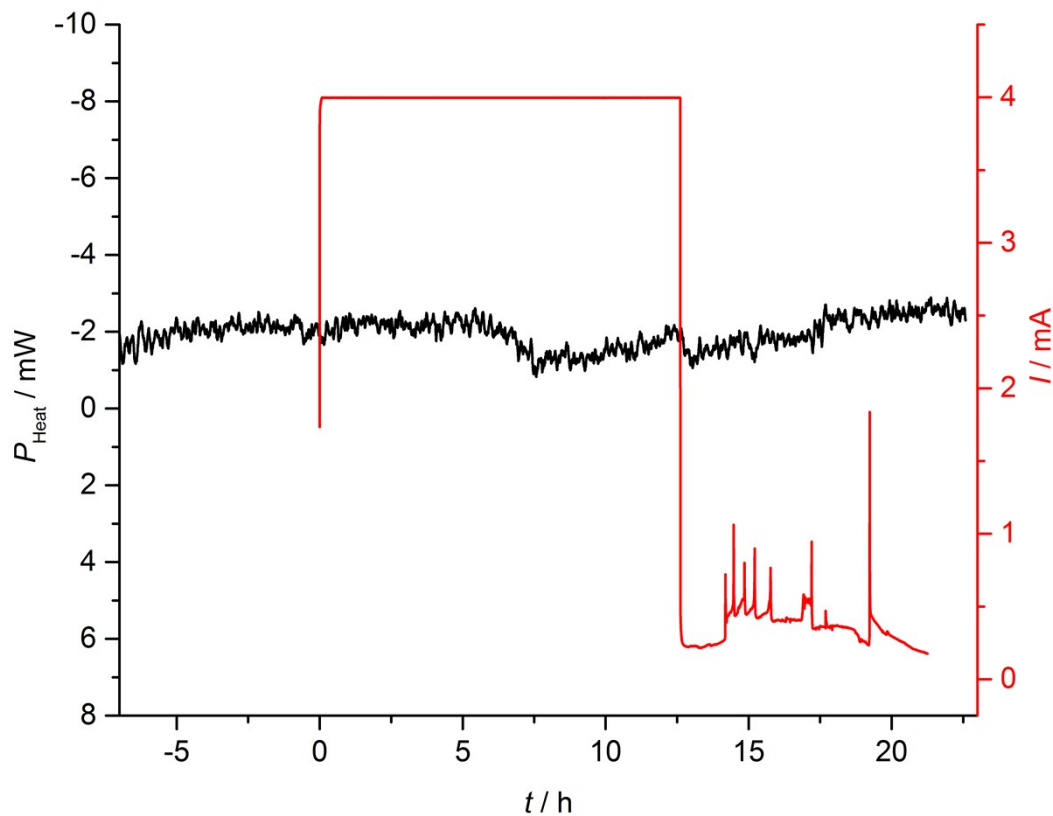


**Figure S4.** galvanostatic experiment with a current of 4 mA but with the heat production rate  $P_{\text{Heat}}$  not affected by electrochemical reactions at the counter electrode. After 12.5 h the current production collapsed due to bubbles formed at the counter electrode that block the ionic path and  $P_{\text{Heat}}$  was again not affected by these changed experimental conditions.

## 2.4 Position calibration of the 2<sup>nd</sup> reference electrode for measurement of the Joule heating contributing to the heat production rate of the bioelectrocalorimeter

To estimate the contribution of Joule heating to the heat production rate it was necessary to consider the full pathway of ion movement leading to a heat flux measurement. Thereby, ion migration occurring in the working electrode compartment as well as in the counter electrode compartment contributed to the measurable Joule heating (Scheme S1 and Scheme 1 in the main article). For calculating  $P_{\text{Joule}}$  the potential between the working electrode and a 2<sup>nd</sup> reference electrode located in the counter electrode compartment needed to be measured (SI 4.2). To evaluate the correct position of this 2<sup>nd</sup> reference electrode, electrochemical experiments described in SI 2.2 with varying 2<sup>nd</sup> reference electrode positions were performed. The diameter of the 2<sup>nd</sup> reference electrode decreased the diameter of the connection tube between working and counter electrode compartment and coincidentally increased the electrolyte resistance within the connection tube. Subsequently, the Joule heating contributing to the overall heat production rate of the reaction vessel increased. These experiments were conducted with a self-made reference electrode ( $d = 3$  mm, Ag/AgCl 3 molL<sup>-1</sup> KCl) allowing a more exact position calibration. First, a potential was applied to the working electrode and a constant current ( $I$ ) and heat production rate ( $P_{\text{Heat}}$ ) were achieved (Figure S5, time period A). Afterwards, the 2<sup>nd</sup> reference electrode was introduced in the counter electrode compartment and the measured  $P_{\text{Heat}}$  increased when the electrode reached too far inside the reaction vessel (Figure S5, time period B). The position of the 2<sup>nd</sup> reference electrode was then raised again to a location where  $P_{\text{Heat}}$  reached again the same constant  $P_{\text{Heat}}$  (similar to  $P_{\text{Heat}}$  during time period A) (Figure S8, time period C). The determined height represents the last point of the counter electrode compartment that contributed to the Joule heating measured by the calorimeter. This position was kept for all further experiments.

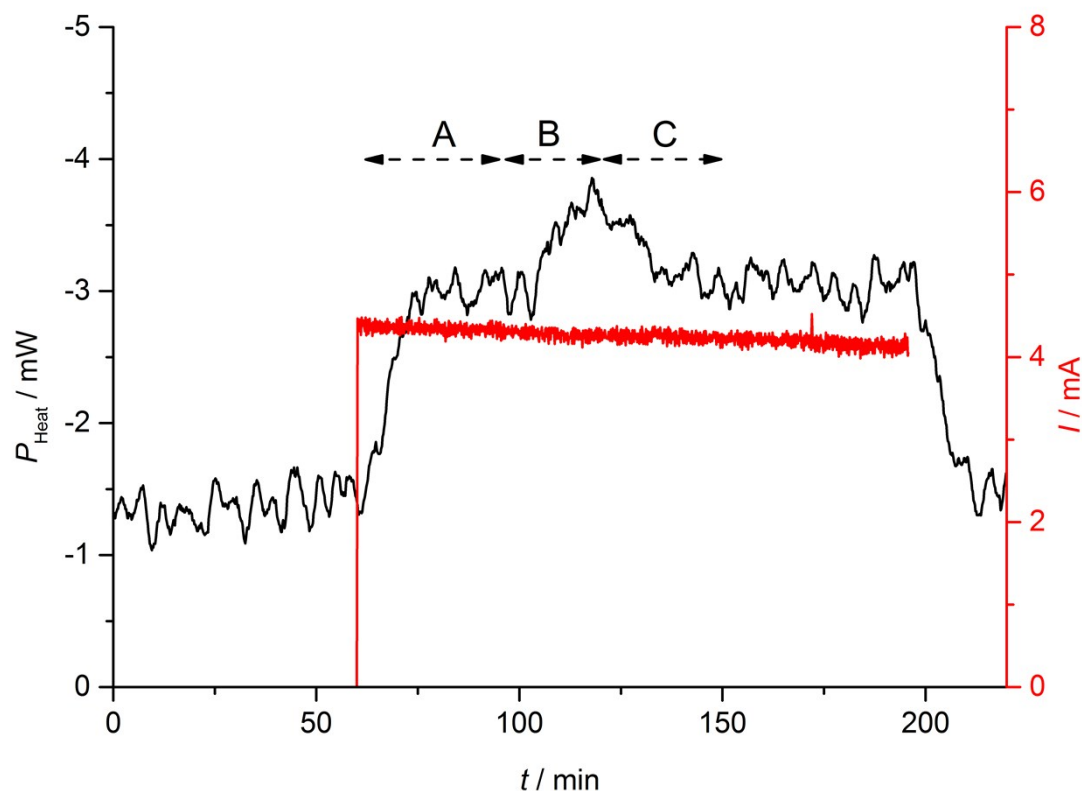


**Figure S5.** Chronoamperometry experiment with 75 mmolL<sup>-1</sup> K<sub>3</sub>[Fe(CN)<sub>6</sub>]/ K<sub>4</sub>[Fe(CN)<sub>6</sub>] and 100 mmolL<sup>-1</sup> NaCl as supporting electrolyte for the position calibration of the 2<sup>nd</sup> reference electrode. The heat production rate ( $P_{\text{Heat}}$ ) and current ( $I$ ) reached a constant level after an oxidative potential ( $E_{\text{WE}} = 0.48$  V) was applied to the working electrode (A). Then, the 2<sup>nd</sup> reference electrode was introduced to the counter electrode compartment and  $P_{\text{Heat}}$  increased due to the increased resistance and resulting higher Joule heating (B). Subsequently, the 2<sup>nd</sup> reference electrode was slowly extricated to identify its correct location not influencing  $P_{\text{Heat}}$  due to increased Joule heating, and  $P_{\text{Heat}}$  reached again the former value without the 2<sup>nd</sup> reference electrode (C).

### 3 Experimental procedure for the determination of the microbial electrochemical Peltier heat

#### 3.1 Setup of the bioelectrocalorimeter

The biological experiments were conducted with the same experimental setup described in SI 2.2.3 but with a graphite rod ( $d = 1$  cm,  $L = 3$  cm,  $A = 10.21$  cm<sup>2</sup>, CP Handels GmbH, Germany) as working electrode (Scheme 1 in the main article). This graphite rod was glued with an epoxy resin (HT2, R&G Faserverbundwerkstoffe, Germany) to a stainless steel wire (Goodfellow GmbH, Germany) with the wire being insulated with a glued PTFE tube (Bohlender GmbH, Germany). The working electrode was placed at a distance of 5 cm to the reference electrode. Furthermore the bioelectrocalorimeter was equipped with a 10 cm stainless steel syringe to enable medium exchange after a growth cycle.

#### 3.2 Cultivation of biofilm anodes

The bioelectrocalorimetric experiments were conducted with secondary biofilm anodes. Primary biofilm anodes were cultivated at 35 °C in a standard bioelectrochemical cell as described in Gimkiewicz *et al.* using a multi-channel potentiostat (MPG-2, Bio-Logic SAS, France).<sup>7</sup> Stainless steel (Goodfellow GmbH, Germany) wired graphite rods (CP Handels GmbH, Germany) served as working electrode ( $d = 1$  cm,  $L = 4$  cm) as well as counter electrode ( $d = 1$  cm,  $L = 6$  cm) and the reference electrode (Ag/AgCl with sat. KCl,  $-0.197$  V vs. SHE, SE 10, Meinsberg Sensortechnik GmbH, Germany) was placed near the working electrode. Primary wastewater ( $V = 12.5$  mL) was used as inoculum and added to the cultivation medium ( $V = 237.5$  mL) as described in Kim *et al.* with 10 mM acetate serving as substrate (i.e. carbon and energy source) being stirred at 120 rpm.<sup>8</sup> Prior to the start of the experiment the solution was purged with nitrogen for 25 min to ensure anaerobic conditions. The working electrode was potentiostatically controlled at 0.4 V during cultivation and intermitted every 24 h for performing cyclic voltammetry ( $E_0 = 0.2$  V,  $E_1 = 0.5$  V,  $E_2 = -0.3$  V,  $n = 3$ ,  $v = 1$  mVs<sup>-1</sup>, working electrode potentials not corrected for  $I \times R$  drop).

#### 3.3 Inoculation of the bioelectrocalorimeter and medium exchange

After cultivating primary biofilm anodes for at least 4 feeding cycles (SI 3.2), a sample of the biofilm was taken by manually using a cell scratcher and stored at  $-20$  °C for T-RFLP genetic analysis (SI 5.2). Another biofilm sample was transferred to 5 mL de-aerated medium, previously described (SI 3.2), with 2 mL of this solution being used to inoculate 198 mL medium (purged for 25 min with nitrogen before) in the bioelectrocalorimeter in order to gain a total working volume of 200 mL with an acetate concentration of 5 mmolL<sup>-1</sup>. The counter electrode compartment was filled with 13.5 mL of the same medium solution but lacking acetate. After each batch of the bioelectrocalorimetric experiment the medium was replaced with a peristaltic pump (Ismatec® Ecoline ISM 1076, Cole-Parmer GmbH, Germany) at a flow rate of 20 mLmin<sup>-1</sup>.

#### 3.4 Calorimetric measurement

The bioelectrocalorimetric experiments were performed with the same conditions described in SI 2.2.3 but at 35 °C. After recording a heat production rate baseline (SI 2.2.4), chronoamperometry experiments ( $E_{WE} = 0.37 \pm 0.10$  V) were conducted using a potentiostat (VSP-300 with a 1A/  $\pm 48$  V booster module, Bio-Logic SAS, France) and interrupted every 96 h for performing cyclic voltammetry ( $E_0 = 0.2$  V,  $E_1 = 0.5$  V,  $E_2 = -0.3$  V,  $n = 3$ ,  $v = 1$  mVs<sup>-1</sup>, working electrode potentials not corrected for  $I \times R$  drop). For more details about additional parameters recorded for the calorimetric analysis of biofilm anodes see SI 4.

## 4 Calculations

#### 4.1 Identifying the heat sources within a bioelectrocalorimeter

In addition to the thermal effects occurring in an electrocalorimeter already described in SI 2.2.2: (i) the electronic Peltier heat flux at the electrode/wire interface and (ii) Joule heat flux caused by the ion migration in solutions ( $P_{\text{Joule}}$ ) further heat fluxes emerge when the reaction vessels hosts biofilm anodes and is operated as bioelectrocalorimeter: (iii) thermal effects due to the overpotential between working electrode and onset potential of the bioelectrocatalytic reaction ( $P_{\text{Over}}$ ), (iv) catabolic heat flux from the anaerobic oxidation of the substrate, here acetate, ( $P_{\text{Cat}}$ ), (v) anabolic heat flux from the build-up of biomass ( $P_{\text{Ana}}$ ) and (vi) the microbial electrochemical Peltier heat flux at the electrode interface ( $P_{\text{mePh}}$ ). Similar to SI 2.2.2 the electronic Peltier heat can be neglected due to its small order of magnitude compared to the other effects. For the studied conditions  $P_{\text{Ana}}$  can also be neglected (see SI 4.5). The remaining heat fluxes  $P_{\text{Cat}}$ ,  $P_{\text{Over}}$  and  $P_{\text{Joule}}$  were individually calculated based on experimental data (SI 4.2-4.4) and summarized in  $P_{\text{Theory}}$  (SI 4.6) for comparison with the measured heat production rate  $P_{\text{Heat}}$ .

#### 4.2 Joule heating

This heat flux ( $P_{\text{Joule}}$ ) is due to solution resistance and ion migration and was derived from the potential difference ( $E_{\text{Joule}}$ ) between the working electrode and the 2<sup>nd</sup> reference electrode (equation 17).<sup>4</sup> The potential  $E_{\text{Joule}}$  was measured with a high ohmic multimeter (VC-20, Conrad Electronic AG, Germany; Scheme 1 in the main article and SI 3.1).

$$P_{Joule} = I^2 R_{Joule} = I^2 \frac{E_{Joule}}{I} = I E_{Joule} \quad (17)$$

### 4.3 Overpotential heating

The overpotential heating ( $P_{Over}$ ) results from the respective overpotential,  $\eta$ , i.e. the difference between the onset potential of the electron transfer reaction of the biofilm anode ( $E_{Onset}$ ) and the applied working electrode potential ( $E_{WE}$ ) at a given current flow (equation 18). By definition the onset potential describes the potential (or the overpotential) at which the electrochemical reaction commences.<sup>9</sup> As soon as the bioelectrochemical reaction starts (i.e. oxidation of outer-membrane c-type cytochromes) electrons cross the electrode interface and current is produced. Therefore, the onset potential rather than the formal potential of the cytochromes should be used to calculate the heat evolving from the applied overpotential. For the performed experiments the onset potential was defined as the mean value of the intersections between the anodic and cathodic current of the third cycle of a cyclic voltammogram with the zero current line (Figure S6). The respective cyclic voltammetry experiments were performed after the redox titration experiments.

$$P_{Over} = \eta I = (E_{WE} - E_{Onset}) I \quad (18)$$

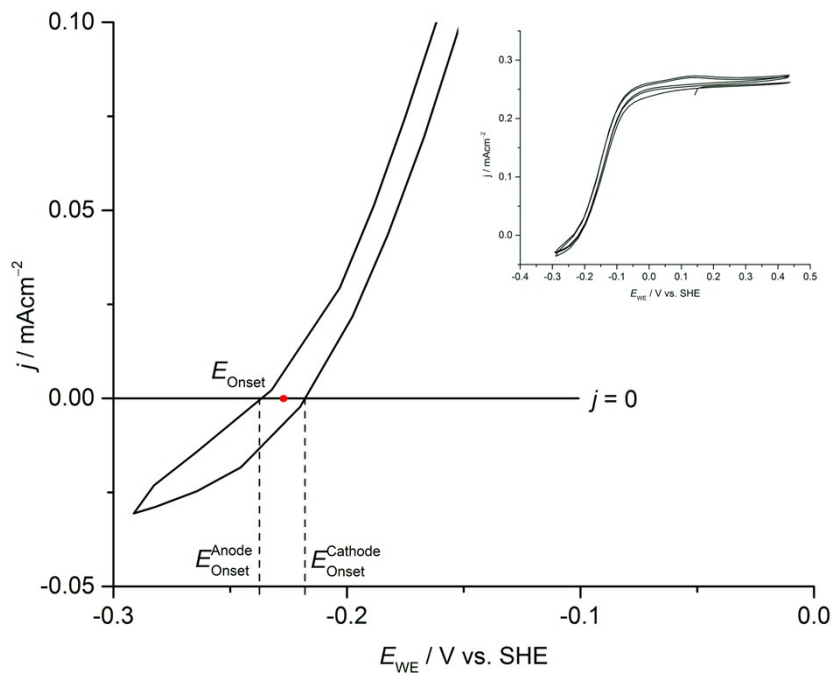


**Figure S6.** Defining the onset potential  $E_{Onset}$  of a biofilm anode for calculating the overpotential heating  $P_{Over}$ . Based on the third cycle of a cyclic voltammetry experiment the potentials of an intersection between the anodic and cathodic current with a zero current line were taken and then the mean value was calculated representing the onset potential. A value of  $E_{Onset} = -0.227$  V was derived in this experiment (red dot). The inset shows a representative voltammogram (with three cycles) of a *Geobacter* spec. dominated biofilm used to determine  $E_{Onset}$  and subsequently for the calculations needed for Figure 2B in the main article.

### 4.4 Catabolic heat due to acetate oxidation

The anaerobic degradation of the substrate acetate by catabolic processes (equation 19) yields not only Gibbs energy which can be used by the bacteria for anabolic and maintenance processes. Also a certain amount of heat is produced or consumed as ubiquitous by-product of any biochemical reaction. This catabolic heat flux ( $P_{Cat}$ ) depends on the standard enthalpy of reaction for the anaerobic acetate oxidation ( $\Delta_R H^0$ ) and the rate of the acetate oxidation ( $r_{AC}$ ).  $\Delta_R H^0$  is calculated with the standard enthalpy of formation  $\Delta_f H^0$  of the reactants (equation 20). According to Hess's law the reaction enthalpy is independent from the reaction path and only the initial and the final state of the reactants determine the reaction enthalpy change. Therefore only the complete anaerobic oxidation was considered and no intermediate metabolic electron transfer steps. The  $\Delta_f H^0$  values were taken from Heijnen *et al.*<sup>10</sup>



$$\begin{aligned}\Delta_R H^0 &= \Delta_f H^0(\text{products}) - \Delta_f H^0(\text{educts}) = 2(-692 \text{ kJmol}^{-1}) \\ &= 246 \text{ kJmol}^{-1}\end{aligned}\quad (20)$$

It results from equation 20 that the anaerobic oxidation of acetate is an endothermic reaction. It was assumed that a mature biofilm (after at least 4 growth cycles) had minimized growth and maintenance processes, in particular during negative potentials steps ( $E_{WE} \leq -0.05$  V) providing only a low driving force (SI 4.5), and as a consequence all 8 electrons gained by the degradation of acetate were transferred to the electrode. Thus, the coulombic efficiency was assumed to be 100% during redox titration experiments. An analysis of the consumption of acetate, e.g. via HPLC, during single steps was not achievable because the different shares of electrons derived from metabolism, reserve substances or electron storage capacity of *Geobacter* spec. dominated biofilms cannot be resolved.<sup>11</sup> Finally, the standard enthalpy of reaction was normalized to a standard enthalpy per transferred moles of electrons ( $\Delta_R H^0_{\text{Electrons}}$ ) by dividing with the number of electrons gained from substrate oxidation:

$$\Delta_R H^0_{\text{Electrons}} = \frac{\Delta_R H^0}{8e^-} = 30.75 \text{ kJmol}^{-1} e^- \quad (21)$$

Since the coulombic efficiency was assumed to be 100% the rate of acetate oxidation normalized to transferred moles of electrons corresponded to the current ( $I$ ) when related to the Faraday constant ( $F$ ):

$$r_{Ac} = \frac{I}{F} \quad (22)$$

Therefrom the heat consumption rate of the catabolic acetate oxidation ( $P_{Cat}$ ) was defined as:

$$P_{Cat} = r_{Ac} \Delta_R H^0_{\text{Electrons}} \quad (23)$$

#### 4.5 Anabolic heat

Low driving force for microbial growth induces a high yield of biomass production but with a distinct decrease in growth rate.<sup>12</sup> Consequently, the heat flux from anabolic and maintenance processes are also reduced. When only slightly higher potentials (compared to the formal potential) were applied to biofilm anodes the driving force for the build-up of biomass was suppressed, especially in mature biofilms showing a steady performance. Thus,  $P_{Ana}$  was disregarded for bioelectrocalorimetric redox titration experiments with mature biofilms for sufficient negative anode potentials (i.e. here defined as  $E_{WE} \leq -0.05$  V).

#### 4.6 Theoretical heat production rate

The heat production rates of the respective heat sources determined in SI 4.2-4.4 were summarized to gain a theoretical heat production rate ( $P_{Theory}$ ) which comprises all - so far known - electrochemical and biological heat sources:

$$P_{Theory} = P_{Joule} + P_{Over} + P_{Cat} \quad (24)$$

#### 4.7 $i \times R$ drop correction of the working electrode potential

The  $i \times R$  drop between working electrode and reference electrode for the cultivation medium in the bioelectrocalorimeter and the following correction of the applied working electrode potential was calculated with the parameters  $L = 5$  cm,  $\sigma = 8.5$  mScm<sup>-1</sup>,  $T = 35^\circ\text{C}$  and a stirring speed of 50 rpm according to the method described in SI 2.2.6.

#### 4.8 Statistical evaluation of the redox titration experiments

The statistical analysis was performed with OriginPro2015G b9.2. 22 full data sets ( $E_{WE} \leq -0.05$  V) from 7 redox titration experiments from 3 biological replicates were available for a statistical analysis of the difference between  $P_{Heat}$  and  $P_{Theory}$  (Figure 2B in the main article). First, the steady state values of  $P_{Heat}$  and  $P_{Theory}$  were related to their respective steady state currents ( $I$ ) and subsequently  $P_{Heat} I^{-1}$  and  $P_{Theory} I^{-1}$  were calculated. After confirmation of (i) normal distribution (Shapiro-Wilk-, Kolmogorov-Smirnov- and Chen-Shapiro-Test, significance level  $\alpha = 0.001$ ), (ii) independency of both sample groups and (iii) homogeneity of the variances; a two-group  $t$  test was performed with the null hypothesis  $H_0: \mu(P_{Heat} I^{-1}) = \mu(P_{Theory} I^{-1})$  and the alternative hypothesis  $H_1: \mu(P_{Heat} I^{-1}) > \mu(P_{Theory} I^{-1})$ . The  $t$  test confirmed that  $P_{Heat} I^{-1}$  and  $P_{Theory} I^{-1}$  were significantly different and subsequently  $H_1: \mu(P_{Heat} I^{-1}) > \mu(P_{Theory} I^{-1})$  was accepted with a significance level  $\alpha = 0.001$ .

## 5 Characterization of biofilm anodes

### 5.1 Cyclic voltammetry

Cyclic voltammetry experiments were performed during chronoamperometry and after redox titration experiments to determine the formal potential of the microbial extracellular electron transfer. Each experiment was conducted with the parameters  $E_0 = 0.2$  V,  $E_1 = 0.5$  V,  $E_2 = -0.3$  V,  $v = 1$  mVs<sup>-1</sup>,  $n = 3$  (working electrode potentials were not corrected for  $i \times R$  drop). The obtained voltammograms showed the typical sigmoidal shape of *Geobacter spec.* dominated biofilm during turnover conditions (Figure S7A), i.e. in the presence of substrate, with the major redox system at a formal potential of  $E_{EET}^f = -0.14$  V (Figure S7B).<sup>13</sup>

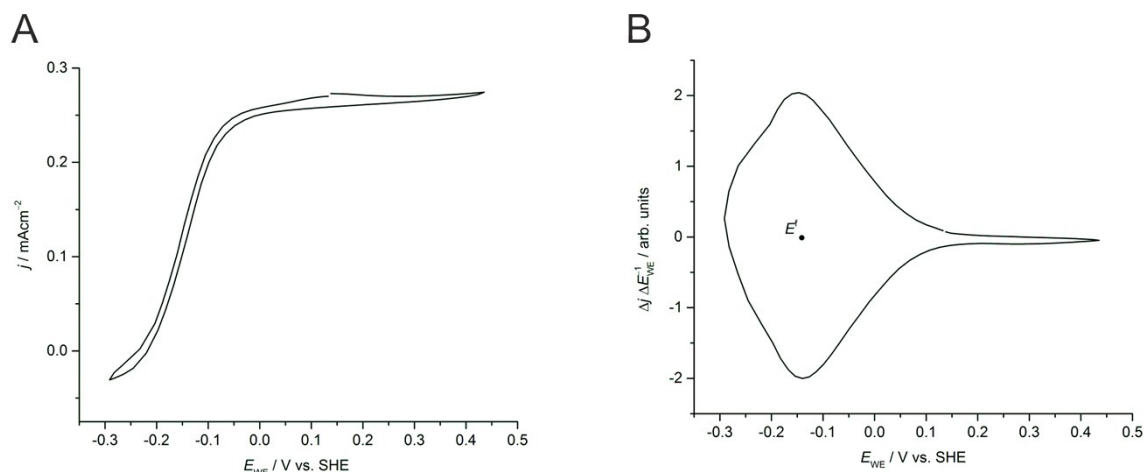


**Figure S7.** Cyclic voltammetry data of a biofilm anodes (A) and its first derivative (B) with a scan rate of 1 mVs<sup>-1</sup>. The sigmoidal shape of the voltammogram and the formal potential of the redox system ( $E_{EET}^f = -0.14$ ) indicated that the biofilm was dominated by *Geobacter spec.* The data was derived from the biofilm used in Figures 1-2 of the main article.

### 5.2 T-RFLP genetic analysis

To identify the community composition, samples were taken from primary biofilms used to inoculate the bioelectrocalorimeter and from secondary biofilms at the end of the calorimetric experiments. Samples were treated as described in Koch *et al.* and a T-RFLP analysis was performed.<sup>14</sup> Based on cloning and sequencing phylogenetic affiliation was possible for terminal restriction fragments (T-RF) of *Geobacter spec.* (Figure S8). The results clearly showed that *Geobacter spec.* were the major member of the electroactive biofilm with an appearance of more than 80%.

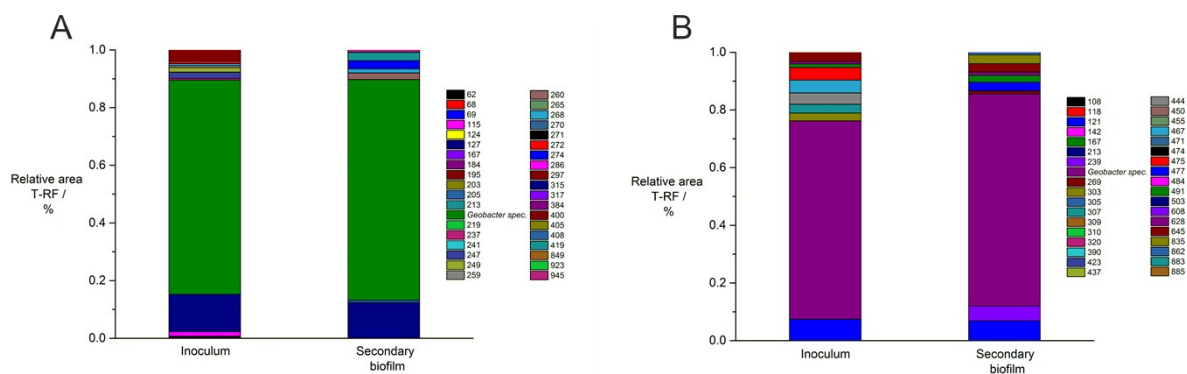


**Figure S8.** T-RFLP analysis of electroactive biofilms used in the bioelectrocalorimeter. Primary biofilm used for inoculation and the secondary biofilm cultivated in the calorimetric setup were analysed after restriction digestion with the enzymes HaeIII (A) and RsaI (B). Both show a dominance of *Geobacter spec.*

### 5.3 Current densities during chronoamperometry experiments

The biofilm anodes were cultivated for at least 4 growth cycles before performing redox titration experiments to assure the maturation of the biofilm anodes and minimizing further growth processes. The achieved peak current densities (Table S2) were representative in comparison with literature.<sup>13</sup>

**Table S2** Peak current densities (in mAcm<sup>-2</sup>) achieved in the first four growth cycles of the biofilm anodes used for the determination of  $I_{lim}$ .

Growth cycle	1 <sup>st</sup>	2 <sup>nd</sup>	3 <sup>rd</sup>	4 <sup>th</sup>
Experiment 1	0.56	0.75	0.78	0.66

Experiment 2	0.24	0.40	0.55	0.48
Experiment 3	0.38	0.48	0.42	0.49
Experiment 4	0.45	0.61	0.50	0.49
Experiment 5	0.53	0.83	0.73	0.62

## 6 References

1. P. Delahay, C. Tobias and C. W. Tobias, *Advances in Electrochemistry and Electrochemical Engineering*, John Wiley & Sons Inc, 1963.
2. K. J. Vetter, *Electrochemical Kinetics: Theoretical Aspects*, Academic Press, 1967.
3. P. Atkins and J. de Paula, *Atkins' Physical Chemistry*, Oxford University Press, 10 edn.
4. P. Boudeville and A. Tallec, *Thermochim. Acta*, 1988, **126**, 221-234.
5. *CRC Handbook of Thermoelectrics*, CRC Press, 1 edn., 1995.
6. P. Vanysek, *CRC Handbook of Chemistry and Physics*, CRC Press LLC, Boca Raton, 82 edn., 2001.
7. C. Gimkiewicz and F. Harnisch, *J. Vis. Exp.*, 2013, DOI: doi:10.3791/50800, e50800.
8. J. R. Kim, B. Min and B. E. Logan, *Appl. Microbiol. Biotechnol.*, 2005, **68**, 23-30.
9. A. J. Bard, G. Inzelt and F. Scholz, *Electrochemical Dictionary*, Springer, 2008.
10. J. J. Heijnen, R. Kleerebezem and M. C. Flickinger, in *Encyclopedia of Industrial Biotechnology*, John Wiley & Sons, Inc., 2009, DOI: 10.1002/9780470054581.eib084.
11. P. S. Bonanni, G. D. Schrott, L. Robuschi and J. P. Busalmen, *Energ. Environ Sci.*, 2012, **5**, 6188.
12. U. von Stockar, T. Maskow, J. Liu, I. W. Marison and R. Patino, *J. Biotechnol.*, 2006, **121**, 517-533.
13. K. Fricke, F. Harnisch and U. Schröder, *Energ. Environ Sci.*, 2008, **1**, 144-147.
14. C. Koch, D. Popiel and F. Harnisch, *ChemElectroChem*, 2014, **1**, 1923-1931.